1996 OMAE — Volume I — Part A, Offshore Technology
ASME 1996

CYCLIC CAPACITY OF TUBULAR BEAM-COLUMNS WITH LOCAL BUCKLING: NUMERICAL AND EXPERIMENTAL STUDIES

B.Skallerud[1], J.Amdahl[2], A.Johansen[3], and O.I.Eide[3]

[1] Div. Applied Mechanics, Norwegian Inst. Techn., N-7034 Norway
[2] Div. Marine Structures, Norwegian Inst. Techn., N-7034 Norway
[3] SINTEF Structural and Environmental Engng, N-7034 Norway

ABSTRACT

The present investigation addresses the cyclic capacity of tubular members subjected to both local and global buckling during cyclic loading. Diameter to thickness ratios of 45 and 60 are studied. The performance of FE models, both a beam model and shell model, is compared to test results in terms of load versus displacement behaviour and energy accumulation. Some problems regarding the prediction of local strain histories in the local buckle zone are pointed out. Damage accumulation models in terms of energy per cycle are discussed, aiming at possible member detachment criteria.

INTRODUCTION

Tubular members are extensively used in offshore steel platforms. Typical diameter to thickness ratios are in the range of 30-80. This ratio indicates the potential for local (shell) buckling. In reassessment of older platforms with revised structural and/or load conditions (cracks, corrosion, dents, increased loads, damage caused by accidental loads), a cyclic nonlinear structural analysis may be required in some cases. Such analyses may confirm whether the redistribution of member forces due to plastic deformations stabilises during the application of the load train due to waves. Furthermore, the accumulated damage in the members during the cyclic load history should be accounted for if member detachment is a failure criterion. Assessment of tubular joints subjected to intense cyclic plastic deformation has been addressed in (Skallerud et al, 1995).

In the present investigation the cyclic capacity of tubular members is discussed. As a part of an ongoing research project test data on the cyclic behaviour of tubular members have been obtained. Members with diameter to thickness ratios of D/t=35,45,60,80 and reduced slenderness ratios of 0.75 and 1 were tested, thus providing data for verification of numerical analyses accounting for both global and local buckling. In this paper FE models using beam elements (USFOS) and shell elements (ABAQUS) are considered for the D/t ratios of 45 and 60. First, some relevant test results are presented. Then the accuracy of simulated load versus displacement and energy absorption are checked. Some problems regarding local buckling and prediction of strains in the local buckle are discussed.

EXPERIMENTAL INVESTIGATION

The tubular members were manufactured from steel plates in 3m long segments with a longitudinal seam weld, and longer members were obtained by girth welding of the segments. The length of the tubular members tested was 3380mm and 5936mm for D/t=45 and 60, respectively. The thickness was 4mm for both geometries. The steel was of type ST52-3N, i.e. a normalised CMn structural steel, typically used in offshore structures. The tensile yield stress, obtained from coupon tests on the actual material, was approximately 410MPa. The tensile strength and fracture strain were approximately 490MPa and 36%, respectively. Some stub-column tests were also carried out for the tube with D/t=60. Figure 1 illustrates the stress-strain behaviour from a tensile (coupon) test and a stub column test. In addition, a Ramberg-Osgood fit to the stub-column curve is plotted. The early yielding due to residual stresses is observed in this curve in contrast to the coupon tensile test.

The axial load was applied with an eccentricity of 4mm to introduce a small 1st order bending moment in the tubular and a preferred direction for global buckling. The imperfections of the tubes in terms of out-of-straightness were very small, in most cases less than 1mm. The longitudinal seam weld was located 90 degrees off the generator subjected to the most severe global/local

buckling in order to have a base material in the local buckle. If the seam weld was located along the top generator, weld material and weld geometry variations may introduce additional scatter in cyclic capcity in terms of cycles to local buckling or through-thickness cracking. Several of the tests were presented by Amdahl et al (1995) in terms of axial load versus axial or transverse displacements.

A test result is plotted in Figure 2a, showing the axial response for a tubular with D/t=45 (denoted B11 subsequently). This test was run in displacement control, consisting of two cycles with a compressive mean displacement of -20mm and an amplitude of approximately 10mm, followed by fully reversed cycles with amplitude 8mm. In the latter block the specimen failed after three cycles due to through-thickness-cracking (t-t-c) in the local buckle region. Note that local buckling occured in the first compressive excursion at a displacement of -12mm as indicated in the figure. Furthermore, the maximum tensile and compressive capacity in the fully reversed cycles is maintained before significant cracking develops. When the t-t-c has developed, the tensile capacity falls rapidly, and a criterion for member failure may be defined on this basis.

Figure 3a depicts the total energy accumulation as a function of axial displacement. From this plot energy range per cycle can be obtained for the two loading blocks, i.e. approximately 2kJ and 5kJ, respectively. In Figure 4a the energy per cycle versus number of cycles to failure for all tubulars with D/t=45 and constant amplitude loading are plotted. The energy per cycle in each block in test B11 corresponds reasonably well with the energy in the constant amplitude loading at the respective mean displacements (tests B1,B5). Hence, the results from these test can be used to check the validity of a linear damage accumulation rule as discussed later.

Figure 2b shows the axial load-axial displacement for test C1, i.e. D/t=60 and number of cycles to t-t-c of 15. Note the bifurcation due to local buckling at a displacement of approximately - 12mm as indicated. Figure3b illustrates the evolution in total energy for this test, with an energy range of about 1.4kJ per cycle. Figure 4b exhibits energy per cycle versus number of cycles to t-t-c for all specimens with D/t=60 (and t=4mm). As in Figure 4a it seems possible to obtain a linear regression curve for cyclic capacity for the actual tubular cross section.

In all of the tests with local buckling very distinct local buckle shapes developed.The characteristics of the local buckle for the D/t=45 and 60 are shown in the insets in Figure 4. For the B tubes the buckle is inwards, and the C tubes buckles outwards in one half-wave.

NUMERICAL SIMULATIONS

Models and formulations

The numerical work was concentrated on the two above described tests B11 and C1(=C2) as these D/t ratios show a response where both global and local buckling govern the behaviour (the series with D/t=35 is dominated by global buckling, the series D/t=80 is dominated by local buckling).

The basic USFOS element was applied in the beam models, with one element per test specimen. Details of the formulation are given elsewhere (e.g. Eberg et al, 1993). In brief, an updated Lagrangian description of motion is used, combined with concentrated plastic hinges at the beam ends. The plastic interaction between bending moments and axial forces is accounted for by means of closed form solutions for the yield surfaces and fully plastic (bounding) surfaces. The size of the yield surface is characterised by the ratio between first yield in extreme fiber and the full plastic capacity. Hence, a nonlinear transition from first yield to fully plastic behaviour is obtained. Furthermore, the yield surface is modified for local buckling according to the monotonic, semi-empirical criterion derived by Taby (1986). Subsequently, the performance of this model is assessed by comparison to test results. Some simulations of the tests were presented by Amdahl et al (1995). In the present study an improved version of the program is applied. By numerical calibration to elasto-plastic column curves an initial imperfection of 0.002*L of sinusoidal shape is employed in the simulation of the tests in order to comply with the design column buckling curves (Hellan et al, 1994). Tthis accountt for the residual stresses and local imperfections in the beam-columns to the extent that the data base includes pipes of the same characteristics as those in the pipes tested. For simulation of tests B11 and C1(=C2), the initial imperfections are 6mm and 11mm, respectively. The remaining parameters for description of the plastic cross section behaviour were based on default values (size of yield surface, plastic transition parameter, size of cyclic yield surface, kinematic hardening rate of the bounding surface).

The ABAQUS program suite (Hibbitt et al, 1995) was utilised for the shell element analyses. A four noded thin shell with reduced integration was used (S4R5), with 5 integration points through thickness. This program also utilises a Lagrangian formulation. Two types of constitutive models were applied, one is based on the stub-column stress-strain curve given by means of discrete points on the curve (note that a good description of the initial material behaviour is obtained, but during load

reversals the model simulates isotropic hardening), the other one is based on a bilinear kinematic hardening model according to the tensile test stress-strain curve (hence, the early reversed yielding due to the Bauschinger effect may be accounted for to some extent), see Figure 1. Figure 5a shows a typical FE mesh. In the central part of the tube the element length is of order shell thickness. Note that the symmetry plane through the beam axis, where global buckling occured, was utilised since this puts few restrictions on the local buckle behaviour. If the symmetry plane normal to the beam axis at midlength is used, one will introduce restraints on the local buckling behaviour due to boundary conditions, either complying with a symmetrical or antisymmetrical local buckle shapes. Therefore, the shell FE models were quite large, with about 10000 degrees of freedom.

The main advantage of the shell model compared to the beam model is the possibility to calculate strain histories in the local buckle region. These strains could be employed in a damage assessment based on a strain range versus number of cycles to failure curve for the actual material, i.e. independent of geometry. Alternatively, the global parameter work per cycle is also assessed subsequently as a possible damage parameter.

Results: Buckling modes from eigenvalue analyses in pre- and post-collapse region

The measured imperfections in the specimen regarding out-of-straightness were less than 1mm, and local shape variations were even less. Only an average measure of local imperfections could be obtained from the measurements. Therefore, the actual local imperfections in the compressed region of the midsection could not be accounted for.

Prior to the cyclic analyses, eigenvectors and eigenvalues from linearised buckling analyses in the pre- and post-collapse region were computed from the shell models in order to investigate variations of local buckling shapes depending on the elastic or inelastic material behaviour. Figure 5b illustrates a typical axial load versus axial displacement behaviour in a shell analysis. Pre-collapse buckling analysis is carried out at load level A, whereas post-collapse buckling analysis is carried out at displacement level B (i.e. before local buckling develops in the nonlinear analysis). These results provide information on possible shapes of local imperfections that may be utilised in the nonlinear cyclic analyses. Note that in the post-collapse region a significant bending moment, prior to local buckling, is introduced at midsection of the tubular. This gives an imperfection due to ovalisation of the cross section analogous to the Brazier effect in pure bending of tubular cross sections (Brazier,1927). This is automatically accounted for in the shell FE analyses.

Figure 6a shows the first three buckling shapes for member B11 (D/t=45) in the pre-collapse region. The two first ones correspond to column buckling, whereas the third contains local (shell) buckling. Figure 6b illustrates the two first local buckling modes in the post-collapse region (at an end shortening of 8mm, prior to occurence of computed local buckling). Note that the first mode is antisymmetrical and the second is symmetrical. The eigenvalues for local buckling in this region is very close. Hence, all of these shapes may be important, depending on the actual local imperfections.

Figure 7a and b show the corresponding plots for specimen C1 (D/t=60) . Interestingly, only the first pre-collapse shape is column buckling, then there are combined modes. In the post-collapse range (at end shortening of 10mm, before bifurcation due to local buckling occurs in the nonlinear analysis), the eigenvalues are very close for the successive antisymmetrical and symmetrical buckling shapes. Note that the buckle wave lengths are much longer for this D/t ratio compared to D/t=45.

Because the eigenvalues are very close in the above analyses, it is not obvious which local imperfection to use according to a single local buckling mode in the nonlinear analyses of the tests. Although a linear combination of several local buckling modes may be utilised for local perturbations of the shell geometry, that approach was not pursued in this investigation.

Results: Load-displacement and energy dissipation

Axial load versus end shortening with or without local buckling in the beam model (USFOS) are plotted for B11 specimen in Figure 8a and c, respectively. Comparing with Figure 2a it is observed that the buckling load is well predicted (approximately 650kN). Ignoring the effect of local buckling overpredicts the compressive load in the post-collapse region and the tension load for the first load block (±20mm±10mm). In the second block (±10mm), the tensile load is accurately predicted, but the compressive capacity is overpredicted somewhat. The simulation accounting for local buckling shows a distinct change of stiffness at -10mm due to local buckling. The magnitude of the post-collapse load is very well predicted, while the tensile load in the first loading block is somewhat overestimated The tensile load in the second loading block is underpredicted, and the compressive load reasonably well predicted.

The corresponding shell analysis (ABAQUS) of B11, utilising the stub-column stress-strain curve as basis for material parameters, are illustrated in Figure 9a. The prediction of the buckling load is good, showing a

bifurcation at -10mm (just as in the beam model), and accurate simulation of the post-local buckling behaviour. In this case, the tensile amplitude in the first loading block is well predicted, and the tensile load in the second block is also reasonable. However, due to overly straightening of the local buckle in the simulation combined with no account of the Bauschinger effect in the constitutive behaviour, the buckling loads in the second loading block is overpredicted. In order to overcome these limitations, the same analysis was performed with a bilinear kinematic hardening material model. This, however, led to significant numerical problems, both in obtaining the global buckling load and local buckling. The predicted local buckling shape for the shell model is given in Figure 10a, with a sharp local buckle, predominantly in outward direction. This mode did not comply with the observed behaviour, where the local buckle occured inwards with a somewhat longer wavelength than in the simulation. This emphasises the difficulty of computing strain histories in the local buckle, for subsequent use in a strain range based damage accumulation assessment.

For the tube with D/t=60 the local buckle ocurred at an end shortening of 12mm and a buckling load of about 650kN, see Figure 2b. The beam model overpredicts the collapse load both with or without account of local buckling (approx. 780kN vs 650kN), see Figure 11a and c. The amplitude of the post-collapse load is quite well predicted in the analysis accounting for local buckling, and the load amplitude is significantly overpredicted in the other analysis. The local buckle initiates at about 10mm end- shortening, followed by a spring back. Both simulations overpredict the maximum force. The deviation of the simulation not accounting for local buckling is not acceptable. The corresponding shell model results are plotted in Figure 9b, showing some overprediction in collapse load (750kN vs 650kN), but the remaining response history is well simulated. It should be noted that the Ramberg-Osgood fit to the stub-column curve in Figure 1 assumes that the elastic modulus is 210000MPa. It is observed, however, that the initial stiffness is slightly less, approximately 188000MPa. If this modulus is applied in the numerical simulations of the C1 test, both the beam and shell model yield a predicted collapse load in good agreement with the test result.

The predicted local buckling shape for this shell model is given in Figure 10b, with a relatively smooth local buckle mostly inwards. This mode did not comply with the observed behaviour, where the local buckle occured outwards with a shorter wavelength than in the simulation. As for the D/t=45 specimen this emphasises the difficulty of computing strain histories in the local buckle for subsequent use in a strain range based damage accumulation assessment.

In summary, it is fair to state that the USFOS model with account of local buckling perforns quite well even in these complex nonlinear regimes. The estimation of collapse load for C1 is improved when using a reduced elastic stiffness according to the initial stiffness in the stub-column test.

Since it is very difficult to predict the exact shape of the local buckle, it is not expected that the computed local strain concentrations in the buckle will be accurate. Hence, a more robust parameter is sought. An alternative approach is possibly to relate damage accumulation to energy dissipation per cycle. It is believed that this parameter is less sensitive to local variations in the strain patterns, as it integrates the work carried out over the entire dented zone. Figure 12a and b show the total energy accumulation for simulation of tests B11 and C1 with the beam model, respectively, whereas Figure 13a and b show the total energy accumulation for the shell models. Comparing the two numerical methods with each other and with the energy absorption in the tests, Figure 3, the following is observed. For B11 the accumulated energy during the first excursion is underpredicted in the shell model, overpredicted in the beam model, but the energy range in the subsequent cycles is quite well predicted with both models. For C1 similar results govern the post-collapse region as for B11, but the range in energy during the cycling is more accurate in the shell model compared to the beam model, where the energy range is underpredicted.

DISCUSSION

The tests showed that tubes are not susceptible to early fracture caused by low cycle fatigue as long as the cross section remains intact. Once local buckling takes place very large strains in the buckled region promotes rapid crack growth. The tests also show that once the crack has grown through the thickness the capacity is significantly reduced. Hence, it is practical to employ t-t-c as a failure criterion. In a cyclic reassessment of a platform such a criterion should be implemented in order to have reliable computations of redistribution of member forces.

There are several challenges associated with a member detachment criterion for cyclically loaded tubulars with global and local buckling. First, from a physical point of view the cyclically loaded shell in the local buckle region is subjected to intense straining leading to low cycle fatigue crack growth. Hence, knowing the local strain history, a crack initiation/growth model could be utilised in calulating the accumulated damage. The tests show that when t-t-c occurs in the local buckle, the tensile and compressive capacity of the member is significantly reduced, hence, t-t-c is employed as failure criterion.

Eq.(1) describes this damage growth rate (Skallerud, 1992)

$$\frac{da}{dn} = A\ (\Delta\varepsilon)^{\beta} \cdot a \qquad (1)$$

If the strain ranges are obtained the number of cycles to failure may be computed. Denoting crack depth by damage variable D, the damage evolution is of the following form

$$D = C\ e^{(\Delta\varepsilon)^{\beta} n},\ C = e^{A} \qquad (2)$$

i.e. an exponential accumulation. Power relationships is also frequently used

$$D = C_1(\Delta\varepsilon)n^{C_2+1} \qquad (3)$$

The experience obtained in the course in this study shows that such a local damage parameter is not very applicable because the strain ranges depend strongly on the actual shape of the local buckle. This is difficult to predict because several local buckle modes are closely located. Alternatively, the global parameter ΔW, i.e. strain energy per cycle, may be proposed. In adopting this damage parameter it is assumed that the energy dissipation in the plastified, locally buckled, cross section governs the strain range in the buckle. If this is the case, ΔW may be substituted in Eqs. (2) and (3). The results of the test have been analysed in view of this model.

Unfortunately, the accumulated energy in the first excursion obscures the data (i.e. prior to intiation of constant amplitude cycling). Obviously, some damage accumulates during this first excursion depending on the maximum end shortening. A possible dependency of in the coefficients C or C1 in Eqs.(2) or (3) on the energy disspiated in the first excursion, $W_{post\text{-}collapse}$ should be investigated. The coefficients may for instance be increasing functions of $W_{post\text{-}collapse}$.

Figure 3 suggests that the relationship between ΔW and N_f may be described by a log-log linear curve. Another question is whether the linear damage accumulation rule, Eq.(4), is applicable.

$$\sum_i \frac{n_i}{N_i(\Delta W_i)} \le 1 \qquad (4)$$

Note that using ΔW as a damage parameter requires reliable computation of the energy, given by

$$\Delta W_i = \int_{t_{i-1}}^{t_i} \int_{V_{phase}} \sigma : \dot{\varepsilon}\ dV dt \qquad (5)$$

where t_i is time to complete cycle no. i. The beam model investigated herein works quite well with respect to energy range. The dissipated energy is efficiently computated by

$$\Delta W_i = \int_{t_{i-1}}^{t_i} S \cdot \dot{v}\ dt \qquad (6)$$

where S denotes the stress resultants in the cross section, vdt the corresponding deformation increment.

From earlier tests tubulars were tested under constant conditions similar to the two sequences described above, i.e. either -20mm ±10mm (test B5) or ±10mm (test B1) (Amdahl et al, 1995), with the number of cycles to failure of 20 and 9, respectively. If a linear summation of damage according to Eqn.(4) is utilised for test B11, the accumulated damage is 2/20 + 3/9=0.43, hence, the test indicates a non-conservatism in the linear rule. But here it should be noted that the damage from the first compressive excursion is not accounted for in the damage accumulation.

So far the cyclic capacity is reported in terms of energy range. The effect of damage accumulation in the first compressive excursion on the number of cycles to through-thickness-cracking will be investigated in a future paper along with the feasibility of the linear damage accumulation model given in Eq.(4). Considering the result from the block loading in test B11, the linear rule does not seem invalidated. The other requirement is accurate computation of energy range in a cross section with local buckling. From the analyses herein, the beam model works quite well, considering its simplifications compared to a shell model.

CONCLUDING REMARKS

Results from cyclic testing of tubular members with D/t ratios of 45 and 60 were compared to numerical simulations obtained with either a beam finite element model or shell finite element models. The global response in terms of axial load versus axial displacement was well predicted with both FE models for the D/t=45 specimen when the beam model accounted for local buckling. The energy accumulation during the cycles was reasonably predicted with both models. The response for D/t=60 specimen was better predicted with the shell model, although both models overpredicted the collapse load. This is partly explained by the significant influence of residual stresses. The energy range was underpredicted with the beam model, whereas this range was reasonably

predicted with the shell model. One motivation for using shell elements was to be able to calculate strain histories in the locally buckled zones, and apply these histories in a strain range based damage accumulation model. However, it proved difficult to determine accurate local buckling shapes in the simulations. Therefore, the global parameter energy per cycle was investigated to some extent. This parameter seems to be feasible as a damage parameter, but further work is needed. One test with block loading (B11) indicates that a linear summation of damage based on energy range is unconservative, when the effect of first compressive excursion is not taken into account.

REFERENCES

Amdahl, J., Skallerud, B., Eide, O.I. and Johansen, A., 1995. "Recent Developments in Reassessment of Jacket Structures under Extreme Storm Loading: Part II - Cyclic Capacity of Tubular Members". OMAE-Proceedings, Vol. 7B, pp. 113-133.

Brazier, L.G., 1927. "On the Flexure of Thin Cylindrical Shells and Other "Thin" Sections". Proc. Royal Soc. Vol. 116, pp. 104-114.

Eberg, E., Hellan, Ø. and Amdahl J., 1993. "The Development of Structural Models for Cyclic Response". OMAE Proceedings, Glasgow.

Hellan, Ø., Moan, T. and Drange, S.O., 1994, "Use of Nonlinear Push-over Analyses in Ultimate Limit State Design and Integrity Assessment of Jacket Structures". BOSS Proceedings, Vol. 3, pp. 323-346.

Hibbitt, Karlson, Sorensen, 1992. "ABAQUS Manuals".

Skallerud, B., 1992, "On the Relationship between Low Cycle Fatigue and Crack Growth Rate Properties in Welded Steel Components", Int. J. Fatigue and Fract. of Engng Mater. Struct., Vol. 15, pp. 43-56.

Skallerud, B., Eide, O.I., Amdahl, J. and Johansen, A., 1995. "On the Capacity of Tubular T-joints Subjected to Severe Cyclic Loading. OMAE Proceedings, Vol. 1B, pp. 133-143.

Taby, J., 1986. "Ultimate and Post-ultimate Strength of Dented Tublar Members". Rep. no. UR-86-50. Div. Marine Struct, NTH.

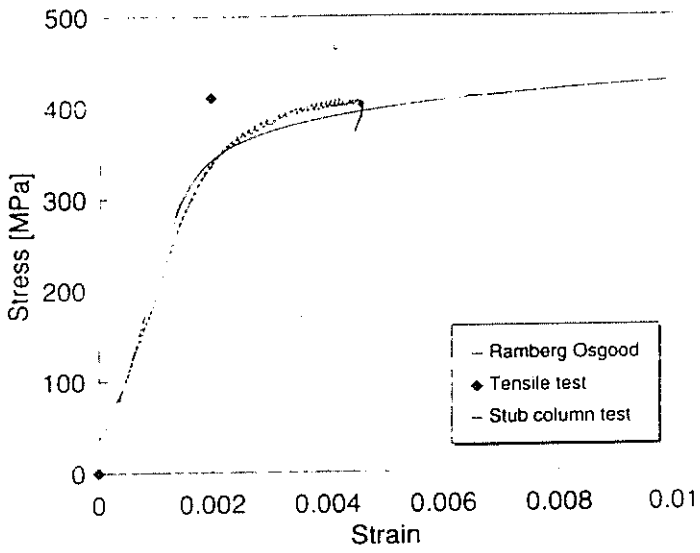

Figure 1 Stress-strain curves.

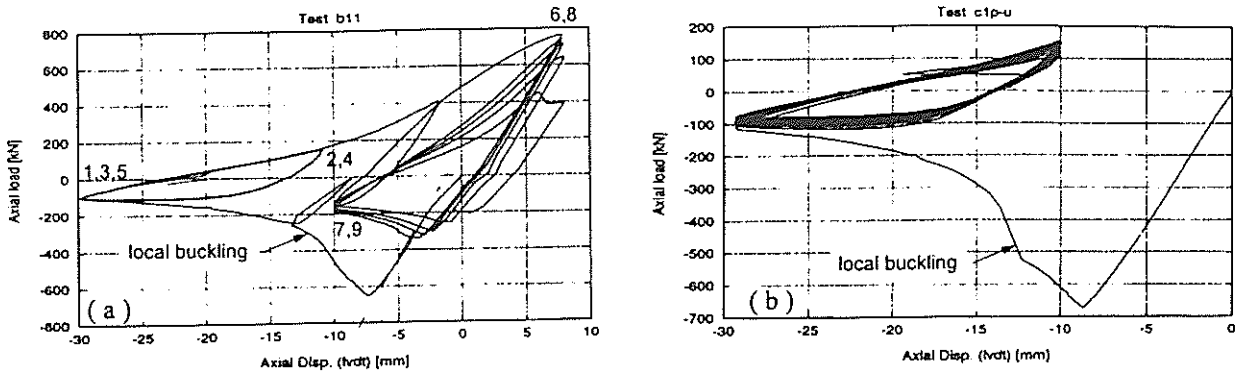

Figure 2 Load-displacement behaviour, test B11, D/t = 45 and C1, D/t = 60, numbers 1-9 represent excursion

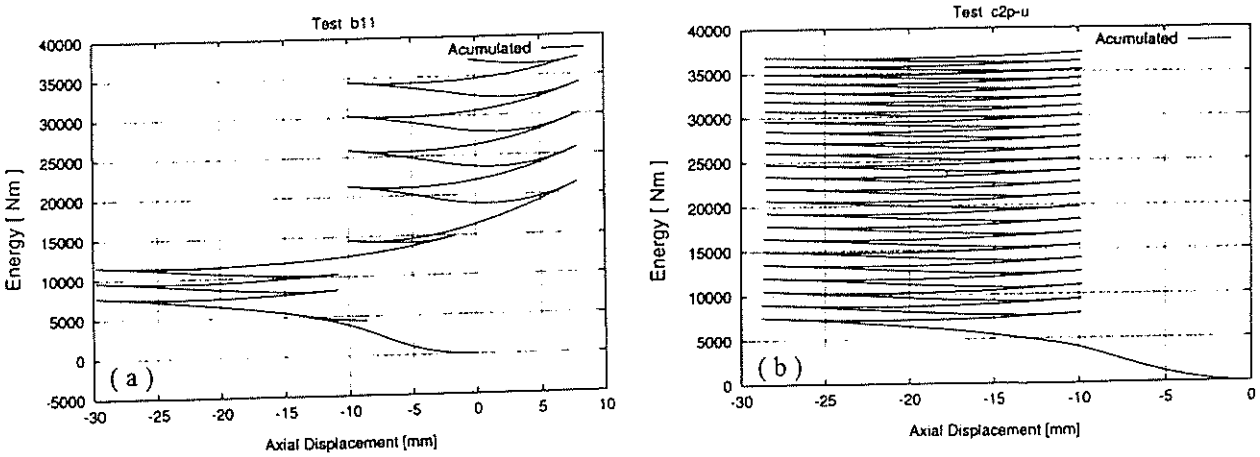

Figure 3 Energy accumulatation in tests B11, C2

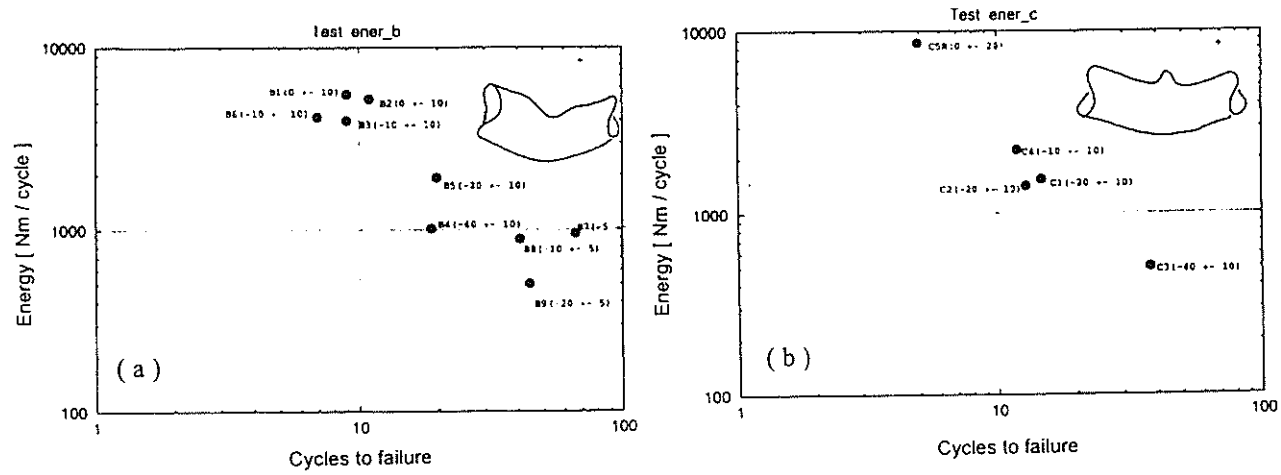

Figure 4 Energy per cycle versus no. cycles to through-thickness-cracking

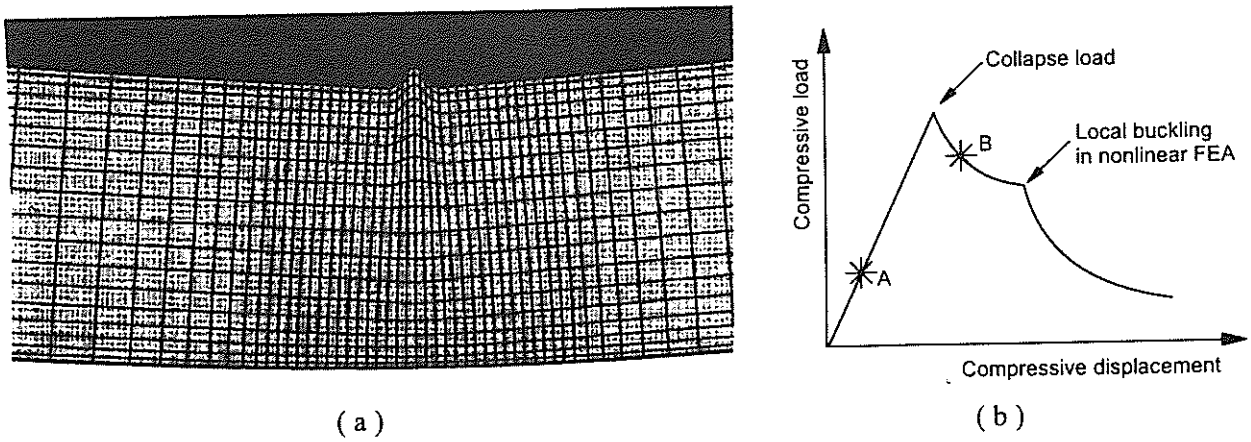

Figure 5 (a) Typical FE-mesh, (b) typical axial load vs axial displ. curve

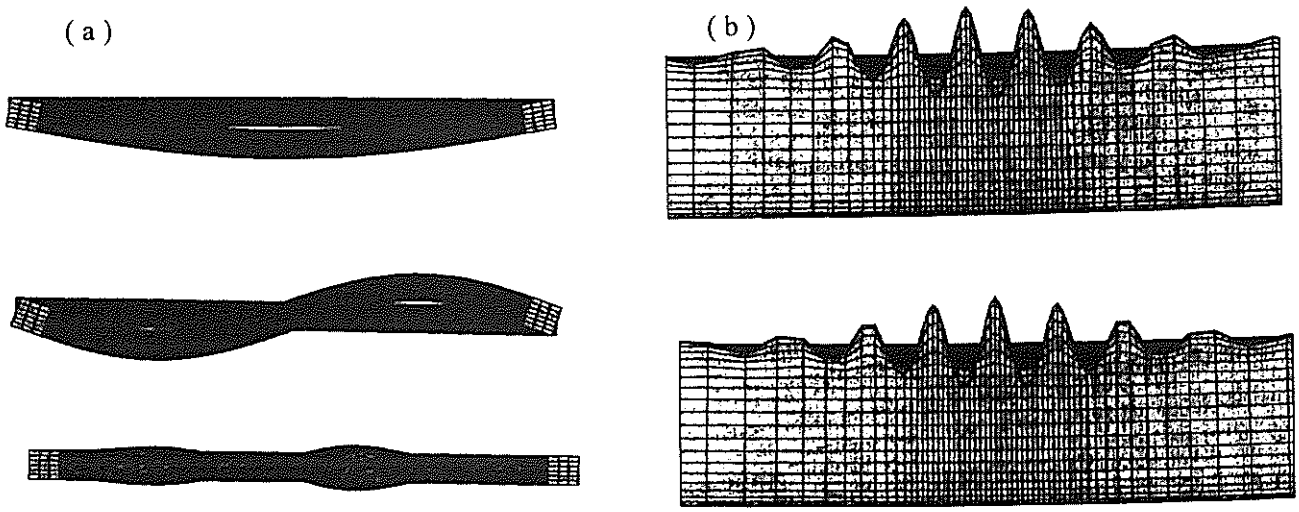

Figure 6 D/t = 45. Global and local buckling modes in (a) pre-, and (b) post-collapse region. (A, B)

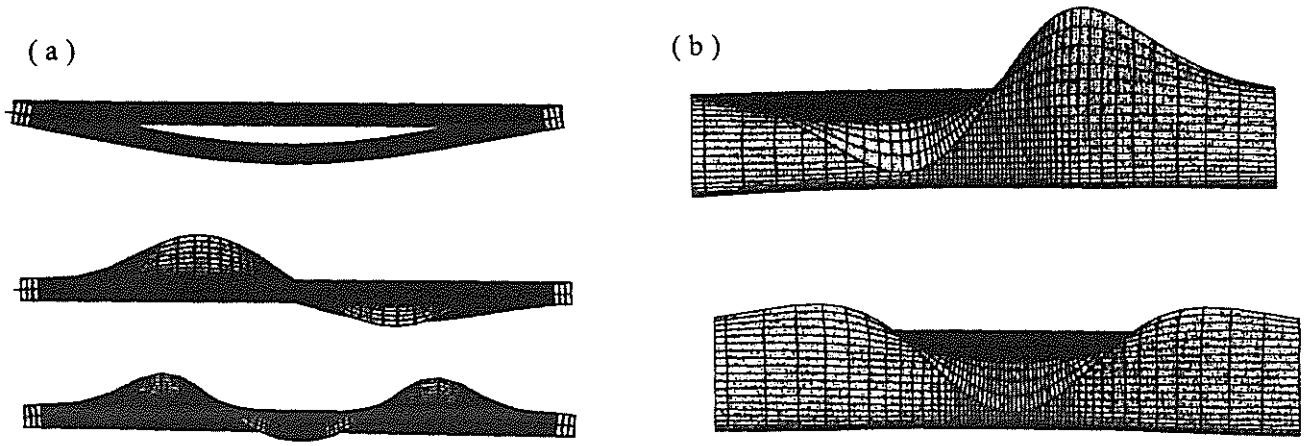

Figure 7 D/t = 60. Global and local buckling modes in (a) pre-, and (b) post-collapse region. (A, B)

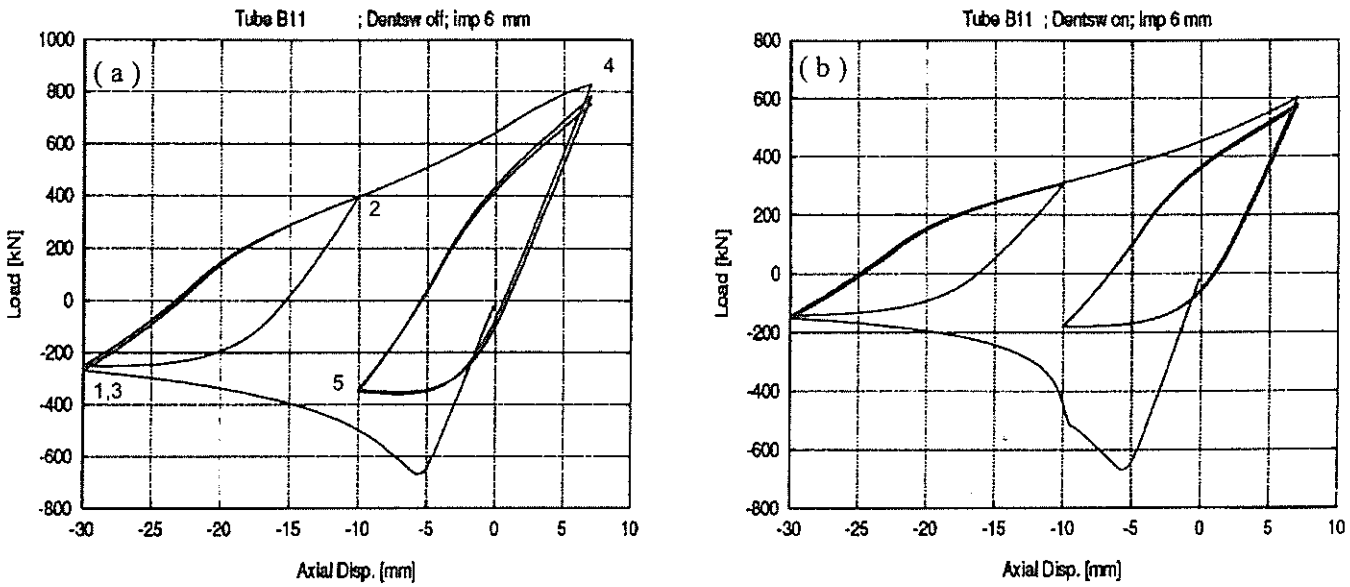

Figure 8 Load-dispacement in beam model without/with local buckling, D/t = 45

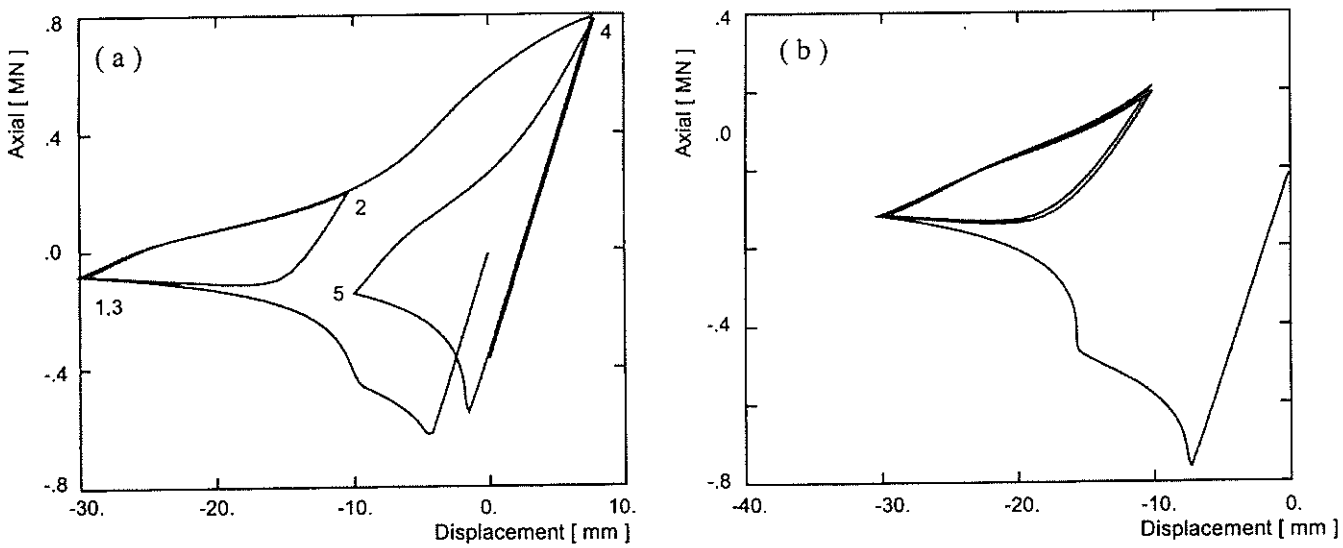

Figur 9 Axial load-displacement in shell model, D/t = 45, 60

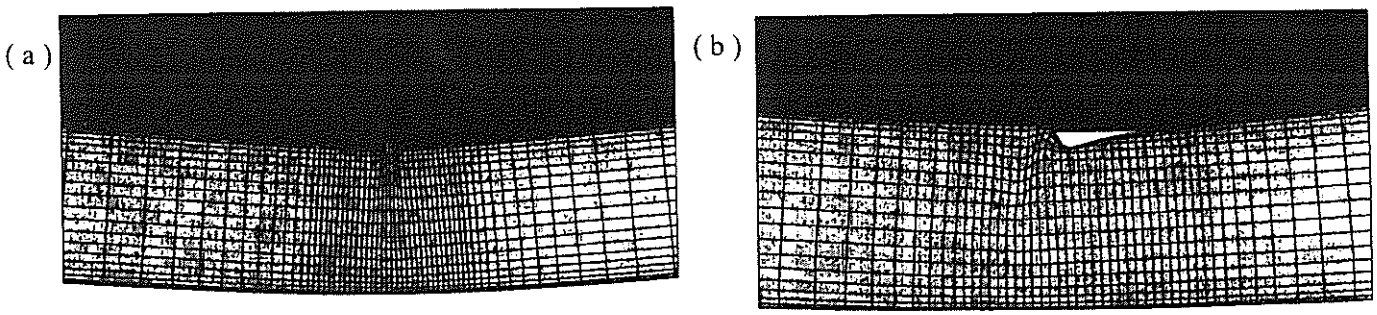

Figure 10 Final local buckling shapes in simulation with shell models, D/t = 45, 60

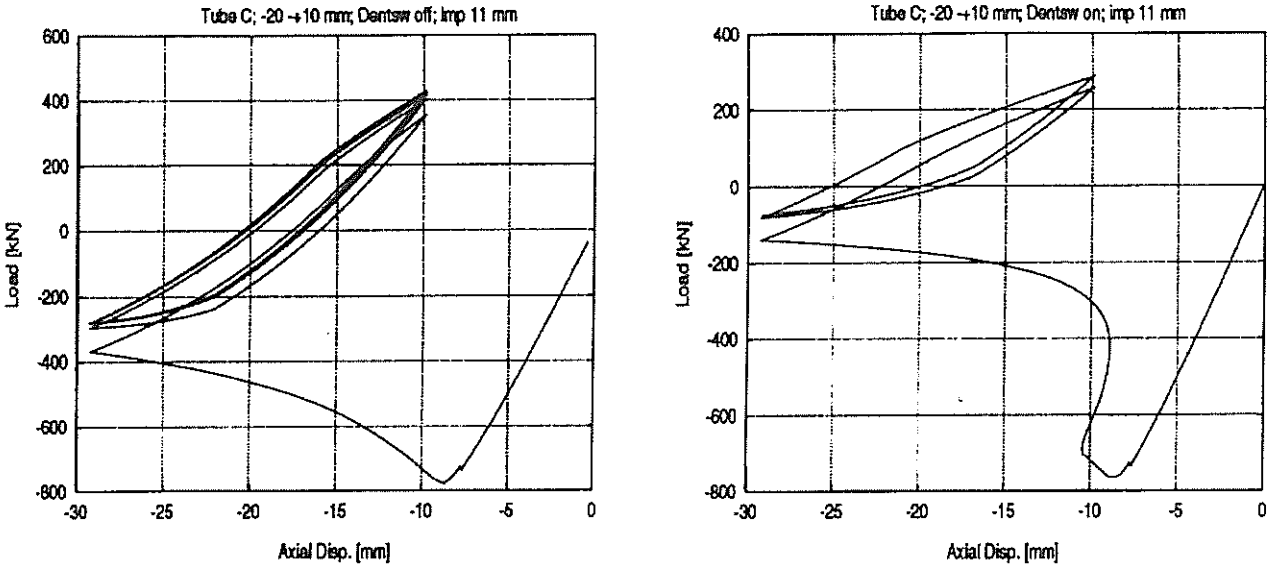

Figure 11 Load-displacement behaviour for beam model without/with local buckling, D/t = 60

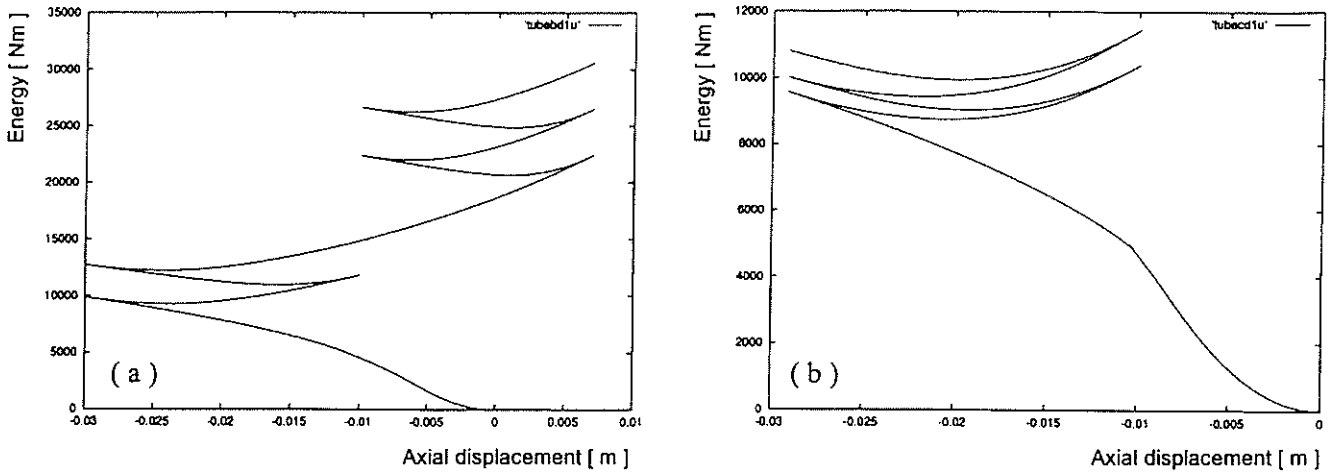

Figure 12 Energy accumualtion, beam models D/t = 45, 60

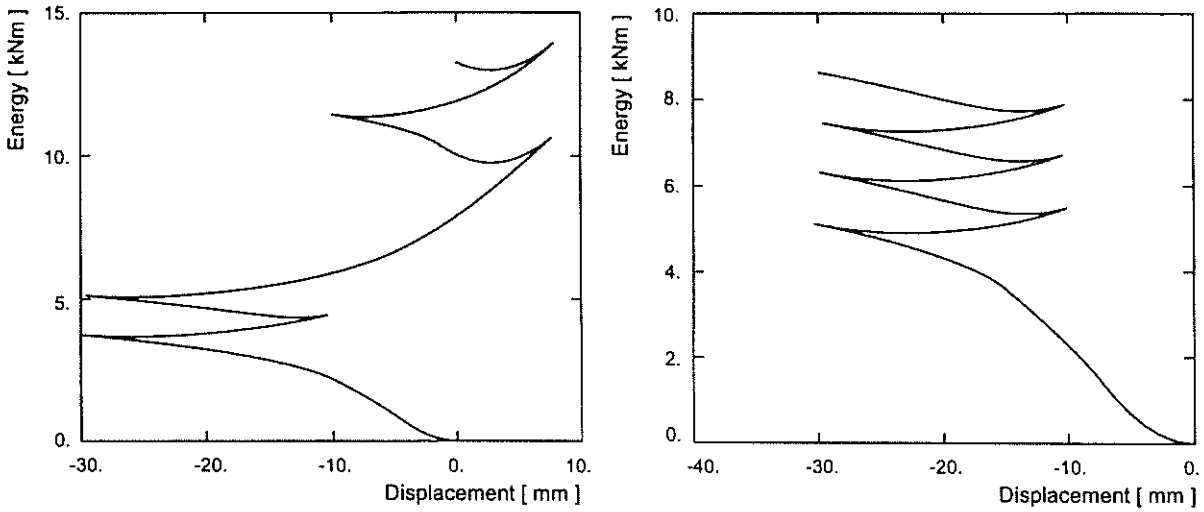

Figure 13 Energy accumualtion, shell models D/t = 45, 60